

Quantification of protein interactions and solution transport using high-density GMR sensor arrays

Richard S. Gaster^{1,2}, Liang Xu³, Shu-Jen Han⁴, Robert J. Wilson³, Drew A. Hall⁵, Sebastian J. Osterfeld⁶, Heng Yu⁶ and Shan X. Wang^{3,5*}

Monitoring the kinetics of protein interactions on a high-density sensor array is vital to drug development and proteomic analysis. Label-free kinetic assays based on surface plasmon resonance are the current gold standard, but they have poor detection limits, suffer from non-specific binding, and are not amenable to high-throughput analyses. Here, we show that magnetically responsive nanosensors that have been scaled to over 100,000 sensors per cm² can be used to measure the binding kinetics of various proteins with high spatial and temporal resolution. We present an analytical model that describes the binding of magnetically labelled antibodies to proteins that are immobilized on the sensor surface. This model is able to quantify the kinetics of antibody-antigen binding at sensitivities as low as 20 zeptomoles of solute.

Affinity-based sensing of DNA hybridization, antigen-antibody binding and DNA-protein interactions play a vital role in basic science research, clinical diagnostics, biomolecular engineering and drug design¹⁻¹⁰. As the state of the art advances, demand for accurate, sensitive, specific, high-throughput and rapid methods for the determination of molecular identities and reaction details places increasing pressure on the evolution of analytical methods¹¹⁻¹⁷. To meet these pressing needs, researchers have turned to nanoscale labels to enhance the limit of detection (LOD) and specificity for detecting low-abundance molecules. Such labels, however, can alter diffusion and steric phenomena. In addition, high throughput or speed requirements often prohibit the use of classical equilibrium methods, so a precise understanding of reaction kinetics, transport phenomena and the implications of surface immobilization becomes critical for extracting meaningful molecular reaction parameters for nanoparticle labelling methodologies. This report addresses these issues and demonstrates that nanoparticle labelled proteins offer unique advantages over label-free methods, making this system very effective for modelling and extracting binding kinetics and analyte transport.

Existing modelling of molecular interactions has predominantly been restricted to label-free binding in solution. Early work by Berg and Stenberg proposed some of the first kinetic models of surface antigen-antibody interactions that explained the new restrictions that labelled reagents introduce on surface reaction kinetics by altering rotational and translational motion¹⁸⁻²⁰. Furthermore, they argued that the use of targets immobilized on sensor surfaces implies that diffusion can become problematic due to the existence of long-range concentration gradients, which can require ligands to traverse macroscopic distances (>100 μm) before reaction. Although many of these details are elaborated by Waite²¹ and Sheehan²², their emphasis on numerical methods precludes the derivation of semi-analytical expressions. Although the binding kinetics of quantum-dot-labelled macromolecules in the liquid phase has been studied with fluorescence cross-correlation spectroscopy^{23,24}, we found no similar literature describing reactions on a sensor surface. Our investigation provides new quantitative

insight into the binding kinetics of labelled macromolecules interacting with targets immobilized on a sensor surface, addressing this gap in the literature.

GMR nanosensor platform and magnetic nanoparticle tags

Our approach uses giant magnetoresistive (GMR) biosensors, an emerging tool for both basic science research and clinical diagnostics. Their superior LOD, multiplex capacity, broad linear dynamic range and real-time readout capabilities make them ideal for kinetic analysis measurements²⁵⁻²⁷. GMR nanosensors, initially used as read head elements in computer hard drives, operate by changing their electrical resistance in response to changes in the local magnetic field²⁸⁻³¹. Recent work has adapted GMR sensors for the detection of biological species in solution by implementing a traditional sandwich assay directly on GMR nanosensors. If a magnetic particle is introduced to label the biomolecule of interest, GMR sensors are capable of highly sensitive DNA and protein detection³²⁻³⁶. This earlier work^{25,26} involved quantifying the amount of protein, but provided little information about the kinetics of the biomolecular reaction. In the current research, we pre-label the soluble ligand with a magnetic nanoparticle (MNP) to monitor the real-time binding kinetics of the ligand-MNP complex to antigens immobilized on sensor surfaces (Fig. 1a). As the antibody-MNP complexes are captured, their magnetic fields induce changes in the electrical resistance of the underlying GMR sensor. Using the rapid, real-time readout of our GMR sensor array²⁵, we can monitor and quantify the kinetics of binding, thus determining the associated kinetic rate constants. Each GMR sensor in the array covers a total area of 100 $\mu\text{m} \times 100 \mu\text{m}$ and comprises 12 parallel GMR sensor stripes that are connected in series six times, producing a total of 72 stripes per sensor (Fig. 1b). Each stripe is 750 nm wide, ~ 20 nm thick and 100 μm in length. Using scanning electron microscopy (SEM), it is possible to resolve nanoparticles bound over each sensor stripe (Fig. 1b, inset).

The MNPs that label the protein or antibody of interest comprise approximately twelve 10 nm iron-oxide cores embedded in a dextran polymer (Fig. 1c), as determined by transmission electron

¹Department of Bioengineering, Stanford University, California 94305, USA, ²Medical Scientist Training Program, School of Medicine, Stanford University, California 94305, USA, ³Department of Materials Science and Engineering, Stanford University, California 94305, USA, ⁴IBM T.J. Watson Research Center, Yorktown Heights, New York 10598, USA, ⁵Department of Electrical Engineering, Stanford University, California 94305, USA, ⁶MagArray Inc., Sunnyvale, California 94089, USA. *e-mail: sxwang@stanford.edu

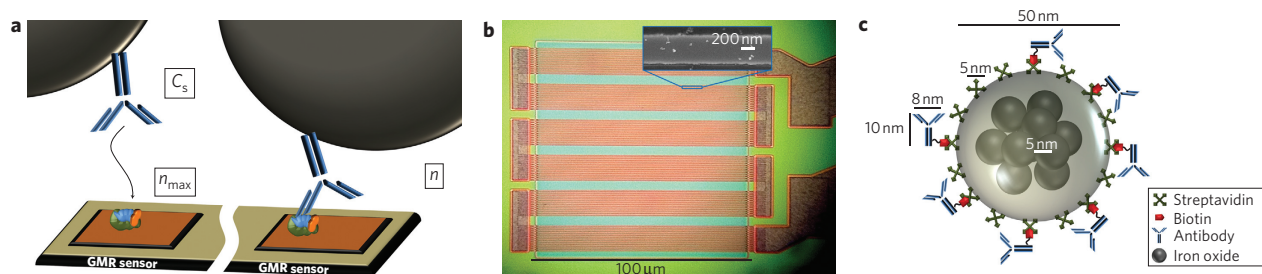


Figure 1 | GMR nanosensor and nanoparticle system for kinetic analysis. **a**, Schematic representation of antibody-antigen binding. On the left, antibody labelled with a magnetic nanoparticle tag in solution at concentration C_s approaches the GMR sensor surface. When not bound, most diffusing magnetically labelled antibodies are too far from the GMR sensor to be detected. Antigens are immobilized on the sensor surface at an initial surface concentration of n_{\max} . Once the magnetically labelled antibody binds to the antigen, as depicted on the right, the magnetic field from the magnetic tag is detected by the underlying, proximity-based GMR nanosensor. The captured antibody-antigen complex surface concentration is n . **b**, Optical micrograph showing the GMR sensor architecture comprising 72 stripes connected in parallel and in series. Inset: SEM image of one stripe of the GMR sensor with several bound magnetic nanoparticle tags. **c**, Schematic representation of a magnetically labelled antibody, drawn to scale. The magnetic tag comprises a dozen iron-oxide cores embedded in a dextran polymer and then functionalized with antibody or receptor.

microscopy (TEM) analysis³⁷. The entire nanoparticle averages 46 ± 13 nm in diameter (from number-weighted dynamic light scattering). Based on the Stokes–Einstein relation, these particles have a translational diffusion coefficient of $\sim 9.3 \times 10^{-12} \text{ m}^2 \text{ s}^{-1}$. The MNPs have a reported zeta potential of -11 mV (ref. 38). These particles are superparamagnetic and colloidally stable, so they do not aggregate or precipitate during the reaction. Importantly, the GMR sensors operate as proximity-based detectors of the dipole fields from the magnetic tags, so only tags within ~ 150 nm of the sensor surface are detected²⁵. Therefore, unbound MNP tags contribute negligible signal in the absence of binding, making this unique nanosensor–MNP system ideal for real-time analysis of kinetic binding process at the sensor surface.

Our GMR assay using MNP labels has several advantages over surface plasmon resonance (SPR), the standard method of monitoring protein binding interactions, which operates by measuring changes in the refractive index of a thin film when unlabelled solute molecules bind to the surface^{39,40}. Although recent studies have attempted to design higher-density SPR instrumentation^{41–43}, their methods typically monitor only a few reactions in parallel, and their LOD and dynamic range are limited to $\sim 25 \text{ ng ml}^{-1}$ and ~ 2 logs, respectively. In contrast, the GMR biosensor array can simultaneously monitor hundreds to thousands of sensors at sensitivities of $\sim 1 \text{ pg ml}^{-1}$ or below and dynamic ranges of 6 log or more²⁶. Furthermore, we have fabricated GMR sensor arrays with 1,008 sensors on a chip area of 1 mm^2 (ref. 44). The calculated feature density is now over 100,000 GMR sensors per cm^2 , the highest density reported to date for biosensor technologies. Each sensor within a subarray is individually addressable by row and column decoders via a shared 6-bit control bus fabricated with state-of-the-art very-large-scale-integration (VLSI) technology. Such highly integrated GMR sensor arrays allow for exceptionally sensitive, massively parallel multiplex monitoring of protein binding kinetics.

Mathematical model of binding kinetics

Given our ability to monitor real-time binding kinetics using highly sensitive and multiplexed nanosensors, we first tested the widely used Langmuir absorption isotherm model, which assumes that there is negligible depletion of reactants and that the concentration of reactants near the surface is the same as that in the bulk. However, this did not adequately describe the binding kinetics in our system (Supplementary Fig. 1). A new model that would accurately describe the binding rates and would give an analytical solution is needed to explicitly describe the microscopic processes and offer insights into the mechanism of the overall reaction. We devised an analytical

model capable of fitting the data with a high degree of generality across a variety of reaction conditions. This new model is capable of fitting real-time binding kinetics data for nanoparticle labelled macromolecules so that one can calculate the molecular association and dissociation rate constants, k_{on} and k_{off} .

Traditionally, protein binding is envisioned as a two-step process in which the target protein or antibody in the bulk solution first enters a surface compartment (reaction zone) via diffusion and flow, and then binds to or escapes from the immobilized targets via the chemical processes of association and dissociation (Supplementary Fig. 2)⁴⁵. If the soluble ligand diffuses slowly, as for a large MNP tag, the diffusion into the reaction zone becomes negligible (see Materials and Methods and Supplementary Figs 2 and 3 for a complete derivation). Therefore, replenishment of soluble antibody–MNP via diffusion from the bulk compartment (bulk zone) to the surface compartment can be assumed to be zero in our model. Accordingly, the rate equation for the traditional two-compartment model can be reduced to the following (see Materials and Methods for derivation):

$$\frac{dn}{dt} = k_{\text{on}} \left(C_0 - n \frac{A}{V} \right) (n_{\max} - n) - k_{\text{off}} n \quad (1)$$

where n is the surface concentration of bound MNP–antibody–antigen complexes that have formed over the sensor, k_{on} is the association rate constant, k_{off} is the dissociation rate constant, C_0 is the bulk concentration of magnetically tagged antibody, n_{\max} is the maximum moles of surface-bound complexes per area, V is the volume of the surface compartment and A is the reaction area (in this case it refers to the surface area of each sensor). The quantity of nA/V is equivalent to the bulk concentration in the reaction zone that would be consumed to produce the surface concentration n , according to mass conservation. Conceptually, the two terms within the parentheses represent the depletion of tagged antibody in the reaction zone and reduction of available surface sites due to binding, respectively.

As both volume and surface concentrations are discussed, we must be aware of the different dimensions: n and n_{\max} are expressed in mol m^{-2} , whereas C_s (Fig. 1a) and C_0 are expressed in mol m^{-3} . Note that n_{\max} is limited by the maximum concentration of close-packed MNPs, not by the maximum concentration of analyte on the surface. So, to exclude steric effects related to MNP crowding on the sensor surfaces, the highest analyte surface concentration tested was significantly lower than the surface concentration of the close-packed antibody–MNP complexes. In addition, by restricting

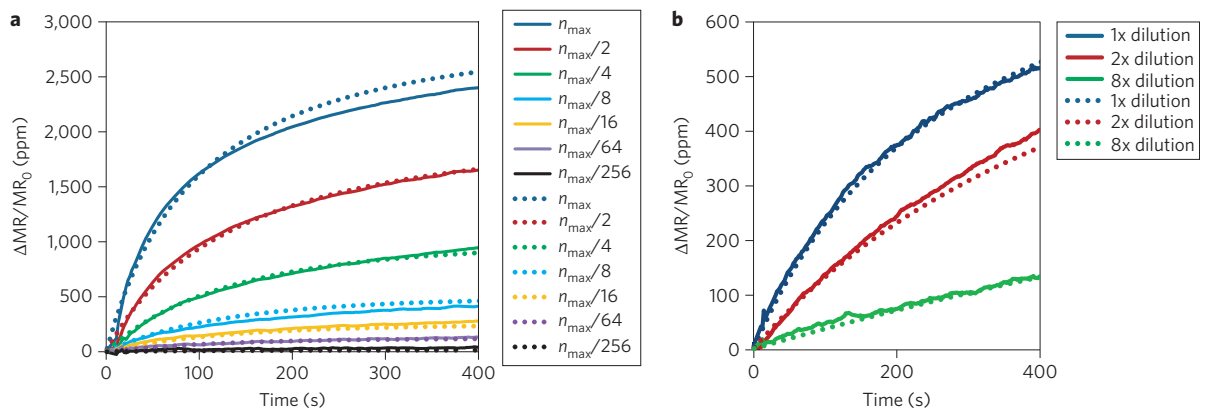


Figure 2 | Comparison of experimentally generated binding curves to kinetic model predictions. **a**, Binding curves for anti-EpCAM antibody binding to EpCAM antigens immobilized on the surface. Dotted lines are predictions using the analytical model in equation (2); solid lines are experimental data obtained for surface loading amounts varying from 5 amol (n_{\max}) to 20 zmol ($n_{\max}/256$) in serial dilutions of 2 \times . The fitting error for all curves in this experiment to curves predicted by the model is $R^2 = 0.98$. **b**, Binding curves for MNP-anti-EpCAM antibody binding to 833 zmol ($n_{\max}/6$) of EpCAM antigen immobilized on the sensor surface. Dotted lines show prediction using the analytical model and solid lines the experimental data obtained for MNP-anti-EpCAM (undiluted, and diluted 2 \times and 8 \times). The fitting error of all curves to the model is $R^2 = 0.96$. The y-axis is presented as changes in magnetoresistance (MR) normalized to the initial MR in ppm.

Table 1 | Comparison of k_{on} for binding of biotin to streptavidin, binding of EpCAM antibody to EpCAM antigen, binding of CEA antibody to CEA antigen and binding of VEGF antibody to VEGF antigen when using the GMR sensor array and SPR.

	GMR sensor ($\times 10^4 \text{ M}^{-1} \text{ s}^{-1}$)	SPR ($\times 10^4 \text{ M}^{-1} \text{ s}^{-1}$)	Literature ($\times 10^4 \text{ M}^{-1} \text{ s}^{-1}$)	Ref.
Biotinylated DNA and streptavidin	467	550	300–4,500	51
EpCAM antigen and antibody	2.5	N/A	3.2–40	52
CEA antigen and antibody	5.0	5.2	3.7–11	53
VEGF antigen and antibody	1.6	N/A	0.5–7	54

For both SPR and GMR sensor experiments, exactly the same antibody pairs were used. Also, each method of kinetic analysis was consistent with the literature. GMR, giant magnetoresistive; SPR, surface plasmon resonance; EpCAM, epithelial cell adhesion molecule; CEA, carcinoembryonic antigen; VEGF, vascular endothelial growth factor.

the amount of protein deposited on the sensor surface to be under this limit, the proteins will be spaced across the sensor at distances greater than one MNP diameter. Therefore, each binding event monitored will be from one antibody on a MNP binding to one antigen on the sensor, and not from multiple antibodies binding to multiple antigens, mitigating avidity issues that may complicate the model.

We further simplify equation (1) by assuming that k_{off} is zero, because antibody–antigen dissociation is typically negligible on the 400–1,000 s timescales of our experiments (Supplementary Fig. 3). Equation (1) now has the following analytical solution (for derivation see Supplementary Materials and Methods):

$$n = n_{\max} \left[\frac{1 - e^{-k_{\text{on}}(C_0 - n_{\max}A/V)t}}{1 - \frac{n_{\max}A}{C_0V} e^{-k_{\text{on}}(C_0 - n_{\max}A/V)t}} \right] \quad (2)$$

If $C_0V \gg n_{\max}A$, which implies a vast excess of solution molecules over available surface sites, the kinetics reduce to Langmuir absorption dynamics (for derivation see Supplementary Materials and Methods), demonstrating that the Langmuir model is merely a special case of our more general analytical model.

Experimental and theoretical binding kinetics measurements

To test this solution, we examined antibody–antigen binding kinetics for the epithelial cell adhesion molecule (EpCAM) using this analytical model, and compared our experimental results to literature values. Anti-EpCAM antibody was selected because it has been formulated into a chemotherapeutic drug, edrecolomab⁴⁶.

In the first set of binding experiments, presented in Fig. 2a, we performed a binding assay of MNP-labelled anti-EpCAM antibody to

surface-bound EpCAM protein. C_0 , n_{\max} , V and A in the model were fixed values determined from dimensions and concentrations, and k_{on} was determined from the best fit of the predicted binding curves to the experimental data. We first performed a binding assay for varying concentrations of surface-bound EpCAM protein at a fixed concentration of MNP–anti-EpCAM antibody complexes. Twofold dilutions were used to prepare a series of sensor surfaces, beginning at a loading mass (the amount of protein that is actually bound to the sensor surface and functional) of 5 amol of EpCAM and diluting sequentially down to 20 zmol. The only parameter that therefore varied between binding curves was n_{\max} ; all other parameters were unchanged. When this one-parameter variation was implemented in the model, each experimental binding curve was fitted accurately (Fig. 2a). The values of the parameters (the undiluted case) were $n_{\max} = 9.5 \times 10^{-10} \text{ mol m}^{-2}$, $C_0 = 6.8 \times 10^{-7} \text{ M}$, $A = 5.4 \times 10^{-9} \text{ m}^2$ and $V = 5.5 \times 10^{-12} \text{ m}^3$. Accordingly, $k_{\text{on}} = 2.5 \times 10^4 \text{ M}^{-1} \text{ s}^{-1}$ fit the data best ($R^2 = 0.98$). In addition, after the MNP–antibody solution was washed away and replaced by antigen-loaded buffer, dissociation constants were calculated by fitting the subsequent data to a basic exponential decay model, $n_{\text{release}}(t) = n_0 e^{-k_{\text{off}}t}$, where n_0 is the surface concentration of bound MNPs at the time of washing (see derivation in Supplementary Materials and Methods). Accordingly, the anti-EpCAM antibody–antigen dissociation constant, k_{off} , was determined to be $2.0 \times 10^{-6} \text{ s}^{-1}$, supporting our assumption that k_{off} is essentially negligible compared to k_{on} .

In a second set of binding experiments, presented in Fig. 2b, each sensor was immobilized with a constant load mass of 833 zmol of EpCAM protein (1/6 of the maximum amount used in Fig. 2a). The concentration of antibody–MNP complex applied to the sensors was varied between undiluted, twofold diluted and eightfold diluted solutions of antibody–MNP complexes (corresponding to

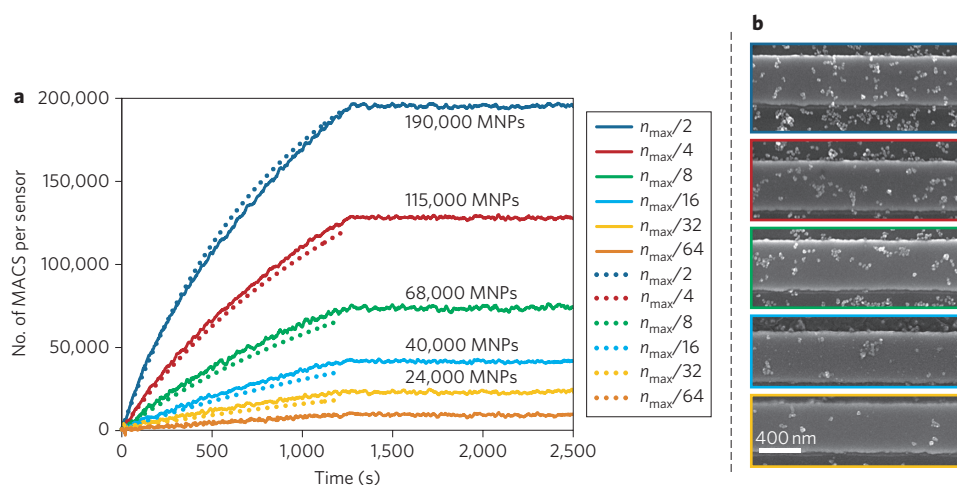


Figure 3 | The kinetic model can predict the number of protein binding events. **a**, By fitting real-time binding curves to the model, it is possible to convert the signal generated from the GMR sensor into an absolute number of magnetic tags bound to the sensor surface. Here, EpCAM protein was loaded onto the sensors at a mass of 2.5 amol (n_{max}) and at masses serially diluted in twofold increments down to 78 zmol ($n_{max}/64$). At least three replica sensors were used for each dilution. After 20 min, incubation with the 20-fold diluted solution of MNP-anti-EpCAM antibody ($C_0/20$), the solution was washed away to terminate the binding reaction. **b**, Subsequently, a small section of the sensors was imaged with SEM (colour-coded boxes represent the different loading masses) to compare the number of MNPs bound in the experiment with that predicted by the model (**a**). The SEM image of $n_{max}/64$ was not shown due to the low surface coverage of MNPs. The number of MNPs indicated above each binding curve in **a** represents the number of MNPs predicted to have bound to each corresponding sensor. Dotted lines are predictions using the analytical model in equation (2) and solid lines are experimental data.

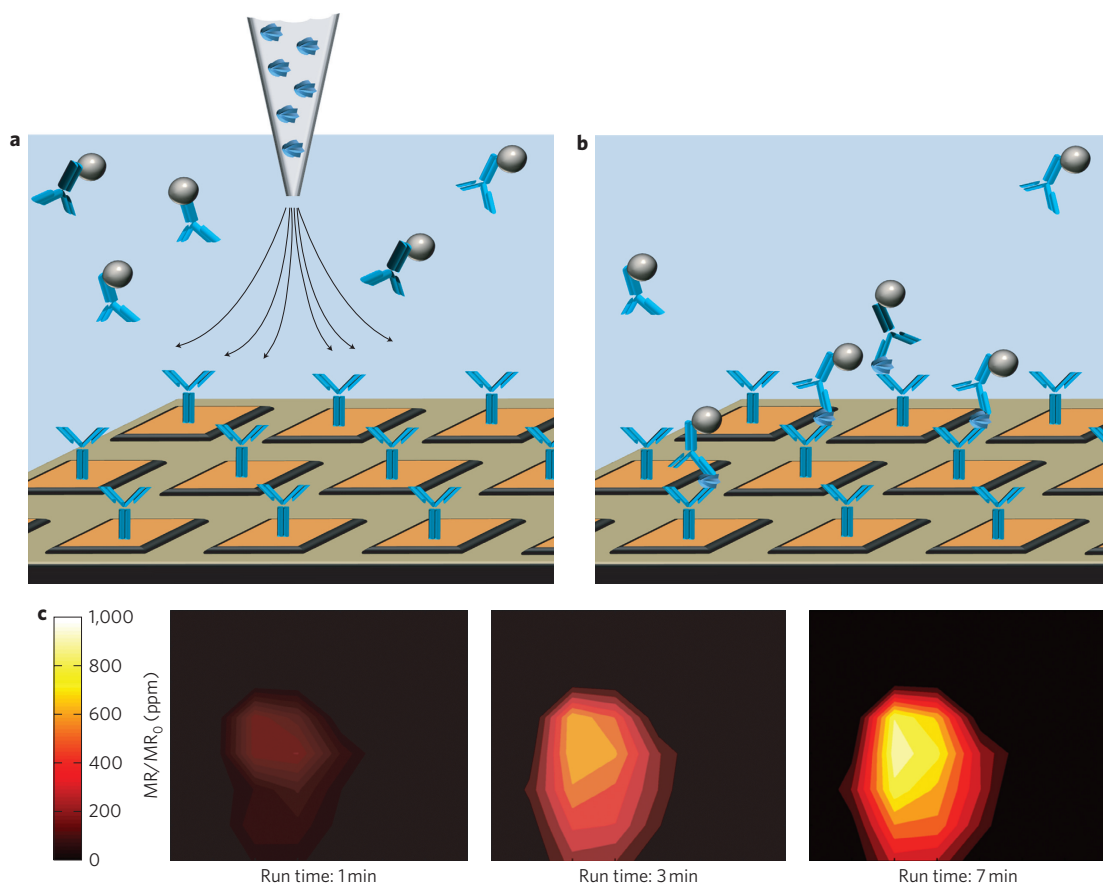


Figure 4 | Visualization of spatiotemporal resolution of the sensor array. **a**, Schematic depicting the GMR sensor array functionalized with monoclonal anti-CEA capture antibody (not to scale). The solution above the sensor array is composed of magnetically labelled anti-CEA detection antibodies. The schematic includes a pipette tip containing a solution of CEA protein before injection. **b**, Once the CEA antigen is introduced into the solution above the sensor array, radial transport of CEA antigen from near the centre of the array is monitored in real time. Magnetically labelled detection antibodies capture CEA protein and bind to anti-CEA antibodies on the GMR sensor surface to form detectable sandwich structures. **c**, Visualization of CEA protein surface concentration at different times using a high-density GMR sensor array. The units of the y-axis are presented in changes in MR normalized to the initial MR in ppm.

C_0 , $C_0/2$ and $C_0/8$ in the model). Because the antibody–antigen interaction should remain the same whether C_0 or n_{\max} is altered, the rate constants describing the interaction above should remain the same across these diverse experiments, as was observed. In fitting the model, we obtained the same k_{on} of $2.5 \times 10^4 \text{ M}^{-1} \text{ s}^{-1}$ ($R^2 = 0.96$), supporting the validity of our analytical model. Furthermore, these results lie within the expected range reported in the literature, confirming both the validity of our kinetic model to predict binding and the accuracy of the results derived (Table 1).

Similar real-time experiments were performed to quantify the binding kinetics for MNP–anti-carcinoembryonic antigen (CEA) antibody to CEA, MNP–anti-vascular endothelial growth factor (VEGF) antibody to VEGF, and MNP–streptavidin to biotin binding kinetics (Supplementary Fig. 4). CEA and VEGF were chosen because they are among the most well-known of clinical tumour markers, and anti-VEGF antibody drugs, such as bevacizumab (Avastin, Genentech/Roche), are highly effective anti-cancer drugs^{46,47}. For anti-CEA antibody, binding and dissociation constants were monitored with the same reagents on both GMR sensors and SPR instruments, and the results were compared (Supplementary Fig. 4c,d). The GMR sensor array and SPR measurements yielded kinetic constants that were consistent with one another and with literature values (Table 1).

SEM analysis confirmed that our analytical system also has the ability to quantify the precise number of proteins captured on each sensor. Thus, by calibrating the GMR signal to an absolute number of magnetic tags bound to the sensor surface, we can derive the mass of protein bound and the signal generated per MNP. To accomplish this, a combination of the previous two experiments was performed and accurately modelled, with EpCAM protein serially diluted in twofold increments, starting at 2.5 amol and ending at 78 zmol, on three to eight replica sensors (Fig. 3a). A 20-fold dilution of the MNP–antibody complexes was subsequently added to all the sensors and the binding kinetics were monitored. After 20 min of incubation time, the solution of magnetically labelled antibody was washed away to terminate the binding reaction, at which point the sensors were imaged by SEM (Fig. 3b). By normalizing the real-time experimental data and fitting it to the model, we were able to convert the sensor signal, measured as a change in magnetoresistance (MR) normalized to the initial MR ($\Delta\text{MR}/\text{MR}_0$), into the number of magnetic tags bound to each sensor. For example, the sensor functionalized with 2.5 amol of EpCAM protein captured 190,000 MNP tags within the duration of the experiment. SEM imaging reveals that the experimental results match with predictions from the kinetic model, thus extending the validity of the model for precisely quantifying the number of tags bound per sensor and determining the number of proteins that bind during a given reaction.

Furthermore, using our models, we estimate that every 150 MNPs produce ~ 1 ppm of the normalized signal. The LOD of our sensors is ~ 20 ppm (defined by the average background signal of a non-complementary antibody coated sensor plus two standard deviations). Therefore, we can detect as few as 0.6 particles per μm^2 . In addition, the model is capable of explaining when saturation of the sensor surface will occur. For example, when 10 amol of protein are deposited on the sensor surface, experimental data show that the sensor surface is approaching saturation as judged by comparing signals at 5 amol and lower (Supplementary Fig. 5). A loading mass of 10 amol is described in the model as n_{\max} being equal to $1.9 \times 10^{-9} \text{ mol m}^{-2}$. The saturation value predicted by the model is thus in close agreement with the maximum surface concentration of the MNPs in a close-packed single layer, $1.0 \times 10^{-9} \text{ mol m}^{-2}$.

Our real-time binding assay and kinetic model has been extended to visualize protein binding events in both space (due to the high density of the array architecture) and time (due to the rapid and real-time readout). As an example, we first immobilized

the same anti-CEA capture antibody across a sensor array. We then added MNP–anti CEA conjugates in solution to the sensor well. On delivery of the CEA antigen, we were able to monitor the movement of CEA protein across the sensor array (Fig. 4a). With this method, we can visualize the binding of soluble CEA protein to each sensor, which is spatially distributed in the array, by means of the MNP–anti-CEA antibody binding (Fig. 4b; Supplementary Fig. 6). In this manner, each sensor monitors the reaction zone above it, so we can investigate protein binding, protein transport and protein dynamics with high spatial and temporal resolution, which is an important and unique development. Such techniques will be applied to monitor localized cell–cell communications via cellular protein secretome analysis in future work.

Discussion and conclusions

We have presented a high-density, highly sensitive, real-time binding assay for quantifying protein binding kinetics and analyte transport at the surface of a biosensor array. Notably, we have also developed a novel analytical kinetics model that provides a precise and physically intuitive description of the dominant processes involved in labelled protein–protein interactions. We have proved that the reduced rate of diffusion, which is consistent with the addition of nanoscale labels, can be used to derive generalizable kinetic binding models with analytical solutions. The combination of the GMR sensor technology and analytical model has enabled us to measure protein binding constants and quantify the number of proteins bound to a given sensor with unprecedented LOD. Furthermore, we have demonstrated the unique benefits of combining our GMR sensor array, kinetic binding assay and analytical model to visualize protein transport in a reaction well.

The tools we have developed can be used broadly in basic science research for understanding receptor–ligand binding interactions involved in signal transduction in cell biology or for profiling the affinity of specific compounds of interest against an entire proteome on a high-density array. In addition, applications to pharmacodynamics via receptor occupancy assays for drug development would open an entirely new and broad field for our technology. MHC-peptide and T-cell receptor interactions could also be studied with exceptional speed and accuracy.

Furthermore, the potential clinical applications of our method are vast, ranging from *in vitro* clinical assay development⁴⁸, to targeted molecular imaging for early cancer diagnostics⁴⁹, to investigating drug on-target and off-target cross-reaction⁵⁰ binding kinetics. In each case, the affinity and cross-reactivity of reagents and targeting probes are critical issues in clinical adoption and can be easily addressed with our platform. In short, our method represents a significant advance in this domain, as it has the potential to provide fundamentally important solutions for both cutting-edge basic science research and clinical practice.

Methods

GMR nanosensor array architecture. The GMR sensor used in our experiment has a bottom spin valve structure of the type Si/Ta(5)/seed layer/IrMn(8)/CoFe(2)/Ru(0.8)/CoFe(2)/Cu(2.3)/CoFe(1.5)/Ta(3), where all numbers in parentheses are in nanometres. Each chip contains an array of GMR sensors, which are connected to peripheral bonding pads by 300-nm-thick Ta/Au/Ta leads. To protect the sensors and leads from corrosion, two passivation layers were deposited by ion beam sputtering. The first thin passivation layer of $\text{SiO}_2(10 \text{ nm})/\text{Si}_3\text{N}_4(20 \text{ nm})/\text{SiO}_2(10 \text{ nm})$ was deposited above all sensors and leads, excluding only the bonding pad area. A thick passivation layer of $\text{SiO}_2(100 \text{ nm})/\text{Si}_3\text{N}_4(150 \text{ nm})/\text{SiO}_2(100 \text{ nm})$ was then deposited on top of the reference sensors and leads, but excluding the active sensors and bonding pad area. The magnetoresistive ratio was $\sim 12\%$ after patterning. The pinning direction of the spin valve was in-plane and perpendicular to the sensor strip. The easy axis of the free layer was set by the shape anisotropy to be parallel with the sensor strip. This configuration allowed the GMR sensors to work at the most sensitive region of their magnetoresistance transfer curves.

As a result of the GMR effect, the resistance of the sensor changed with the orientation of the magnetization of the two magnetic layers, which were separated by

a copper spacer layer:

$$R(\theta) = R_0 - \frac{1}{2} \delta R_{\max} \cos \theta \quad (3)$$

where R_0 is the resistance under zero magnetic field, δR_{\max} is the maximum resistance change and θ is the angle between the magnetization of the two magnetic layers. In the bottom spin valve structure, the magnetization of the bottom magnetic layer (pinned layer) was pinned to a fixed direction, and the magnetic orientation of the top magnetic layer (free layer) could rotate freely with the external magnetic field. As a result, the stray field from the magnetic labels could change the orientation of the free layer magnetization and therefore change the resistance of the sensor.

Magnetic labels. The magnetic labels were commercial magnetic nanoparticles from Miltenyi Biotech., referred to as 'MACS'. Each MACS particle was a cluster of 10 nm Fe_2O_3 nanoparticles held together by a matrix of dextran. Owing to the small size of the Fe_2O_3 nanoparticles, the MACS particle was superparamagnetic, with a hydrodynamic diameter of ~ 46 nm, and contained $\sim 10\%$ magnetic material (wt/wt). MACS particles could be functionalized with specific affinity molecules corresponding to the analyte being studied. For EpCAM (CEA, VEGF) experiments, the MACS particles were functionalized with anti-EpCAM (CEA, VEGF) antibodies; for biotin-streptavidin experiments, the MACS particles were functionalized with streptavidin.

Surface chemistry. The sensor surface was first cleaned using acetone, methanol and isopropanol, and subsequently exposed to oxygen plasma for 3 min. A 2% (wt/vol) polyallylamine solution in Milli-Q water was applied to the sensor for 5 min. The chips were then rinsed with Milli-Q water and baked at 150°C for 45 min. A 10% (wt/vol) solution of 1-ethyl-3-(3-dimethyl aminopropyl) carbodiimide hydrochloride and 10% (wt/vol) solution of *N*-hydroxysuccinimide were then added to the sensor surface at room temperature for 1 h, after which the sensor was rinsed and dried. Capture protein EpCAM (960-EP-050 from R&D Systems), CEA (4128-CM-050 from R&D Systems) or VEGF (293-VE165 from R&D Systems) or capture antibody to EpCAM (ab20160 from Abcam or 960 from R&D), CEA (5910 from BiosPacific) or VEGF (ab69479 from Abcam) was robotically deposited (Sciencion sciFlexarray from BioDot) over each sensor in 360 pl droplets three times (total volume of ~ 1 nl). To monitor reproducibility, three to eight sensors, randomly distributed across the GMR sensor array, were incubated with the same capture protein. The control sensors were immobilized in a similar fashion with either bovine serum albumin (BSA) at 1 mg ml^{-1} or a non-complementary antibody (typically anti-survivin antibody, H0000332-P01 from Novus Biologicals, LLC) at $500\text{ }\mu\text{g ml}^{-1}$. Finally, the entire surface of the sensor array was blocked with 1 mg ml^{-1} of BSA in phosphate buffered saline for 30 min.

Kinetic assay. After the sensor surface was functionalized with the appropriate capture protein, the GMR sensor array was placed in the test station. The BSA blocking buffer was washed away and a $50\text{ }\mu\text{l}$ solution of the magnetically labelled detection antibody (described above) was added to the reaction well. The GMR sensor array was monitored in real time as the magnetically labelled detection antibodies bound to the corresponding surface-immobilized proteins. The binding curves, unique to each protein, were then plotted, and the binding constants could be determined. An assay was typically run for ~ 5 min.

Received 29 December 2010; accepted 8 March 2011;
published online 10 April 2011

References

- Schena, M., Shalon, D., Davis, R. W. & Brown, P. O. Quantitative monitoring of gene expression patterns with a complementary DNA microarray. *Science* **270**, 467–470 (1995).
- MacBeath, G. & Schreiber, S. L. Printing proteins as microarrays for high-throughput function determination. *Science* **289**, 1760–1763 (2000).
- Zheng, G., Patolsky, F., Cui, Y., Wang, W. U. & Lieber, C. M. Multiplexed electrical detection of cancer markers with nanowire sensor arrays. *Nature Biotechnol.* **23**, 1294–1301 (2005).
- James, L. C. & Tawfik, D. S. Structure and kinetics of a transient antibody binding intermediate reveal a kinetic discrimination mechanism in antigen recognition. *Proc. Natl Acad. Sci. USA* **102**, 12730–12735 (2005).
- LaBaer, J. & Ramachandran, N. Protein microarrays as tools for functional proteomics. *Curr. Opin. Chem. Biol.* **9**, 14–19 (2005).
- Park, J. *et al.* A highly sensitive and selective diagnostic assay based on virus nanoparticles. *Nature Nanotech.* **4**, 259–264 (2009).
- Hudson, P. J. & Souriau, C. Engineered antibodies. *Nature Med.* **9**, 129–134 (2003).
- Schrama, D., Reisfeld, R. A. & Becker, J. C. Antibody targeted drugs as cancer therapeutics. *Nature Rev. Drug Discov.* **5**, 147–159 (2006).
- Sinensky, A. K. & Belcher, A. M. Label-free and high-resolution protein/DNA nanoarray analysis using kelvin probe force microscopy. *Nature Nanotech.* **2**, 653–659 (2007).
- Haab, B. B., Dunham, M. J. & Brown, P. O. Protein microarrays for highly parallel detection and quantitation of specific proteins and antibodies in complex solutions. *Genome Biol.* **2**, research0004.1–research0004.13 (2001).
- Wilson, W. D. Analyzing biomolecular interactions. *Science* **295**, 2103–2105 (2002).
- Bornhop, D. J. *et al.* Free-solution, label-free molecular interactions studied by back-scattering interferometry. *Science* **317**, 1732–1736 (2007).
- Stern, E. *et al.* Label-free biomarker detection from whole blood. *Nature Nanotech.* **5**, 138–142 (2010).
- Squires, T. M., Messinger, R. J. & Manalis, S. R. Making it stick: convection, reaction and diffusion in surface-based biosensors. *Nature Biotechnol.* **26**, 417–426 (2008).
- Ramachandran, N. *et al.* Self-assembling protein microarrays. *Science* **305**, 86–90 (2004).
- Patolsky, F. *et al.* Electrical detection of single viruses. *Proc. Natl Acad. Sci. USA* **101**, 14017–14022 (2004).
- Patolsky, F. & Lieber, C. M. Nanowire nanosensors. *Materials Today* **8**, 20–28 (2005).
- Berg, H. & Purcell, E. Physics of chemoreception. *Biophys. J.* **20**, 193–219 (1977).
- Berg, O. G. & von Hippel, P. H. Diffusion-controlled macromolecular interactions. *Annu. Rev. Biophys. Biophys. Chem.* **14**, 131–160 (1985).
- Stenberg, M. & Nygren, H. Kinetics of antigen–antibody reactions at solid–liquid interfaces. *J. Immunol. Methods* **113**, 3–15 (1988).
- Waite, B. A. & Stewart, J. D. An idealized dynamical model of simple diffusional interactions between macromolecules and between macromolecules and surfaces. *Math. Biosci.* **114**, 173–213 (1993).
- Sheehan, P. E. & Whitman, L. J. Detection limits for nanoscale biosensors. *Nano Lett.* **5**, 803–807 (2005).
- Swift, J. L. & Cramb, D. T. Nanoparticles as fluorescence labels: is size all that matters? *Biophys. J.* **95**, 865–876 (2008).
- Röcker, C., Pötzl, M., Zhang, F., Parak, W. J. & Nienhaus, G. U. A quantitative fluorescence study of protein monolayer formation on colloidal nanoparticles. *Nature Nanotech.* **4**, 577–580 (2009).
- Osterfeld, S. J. *et al.* Multiplex protein assays based on real-time magnetic nanotag sensing. *Proc. Natl Acad. Sci. USA* **105**, 20637–20640 (2008).
- Gaster, R. S. *et al.* Matrix-insensitive protein assays push the limits of biosensors in medicine. *Nature Med.* **15**, 1327–1332 (2009).
- Gaster, R. S., Hall, D. A. & Wang, S. X. nanoLAB: an ultraportable, handheld diagnostic laboratory for global health. *Lab Chip* **11**, 950–956 (2011).
- Baibich, M. N. *et al.* Giant magnetoresistance of (001)Fe/(001)Cr magnetic superlattices. *Phys. Rev. Lett.* **61**, 2472–2475 (1988).
- Barnas, J., Fuss, A., Camley, R., Grünberg, P. & Zinn, W. Novel magnetoresistance effect in layered magnetic structures: theory and experiment. *Phys. Rev. B* **42**, 8110–8120 (1990).
- Prinz, G. A. Magneto-electronics. *Science* **282**, 1660–1663 (1998).
- Wolf, S. A. *et al.* Spintronics: a spin-based electronics vision for the future. *Science* **294**, 1488–1495 (2001).
- Mulvaney, S., Myers, K., Sheehan, P. & Whitman, L. Attomolar protein detection in complex sample matrices with semi-homogeneous fluidic force discrimination assays. *Biosens. Bioelectron.* **24**, 1109–1115 (2009).
- Baselt, D. R. *et al.* A biosensor based on magnetoresistance technology. *Biosens. Bioelectron.* **13**, 731–739 (1998).
- Sandhu, A. Biosensing: new probes offer much faster results. *Nature Nanotech.* **2**, 746–748 (2007).
- Koets, M., van der Wijk, T., van Eemeren, J., van Amerongen, A. & Prins, M. Rapid DNA multi-analyte immunoassay on a magneto-resistance biosensor. *Biosens. Bioelectron.* **24**, 1893–1898 (2009).
- Xu, L. *et al.* Giant magnetoresistive biochip for DNA detection and HPV genotyping. *Biosens. Bioelectron.* **24**, 99–103 (2008).
- Koh, A. L. & Sinclair, R. TEM studies of iron oxide nanoparticles for cell labeling and magnetic separation. Technical Proceedings of the 2007 NSTI Nanotechnology Conference and Trade Show, 101–104 (2007).
- De Palma, R. *et al.* Magnetic particles as labels in bioassays: interactions between a biotinylated gold substrate and streptavidin magnetic particles. *J. Phys. Chem. C* **111**, 12227–12235 (2007).
- Malmqvist, M. Biospecific interaction analysis using biosensor technology. *Nature* **361**, 186–187 (1993).
- Katsamba, P. S. *et al.* Kinetic analysis of a high-affinity antibody/antigen interaction performed by multiple Biacore users. *Anal. Biochem.* **352**, 208–221 (2006).
- Lausted, C., Hu, Z. & Hood, L. Quantitative serum proteomics from surface plasmon resonance imaging. *Mol. Cell Proteomics* **7**, 2464–2474 (2008).
- Rich, R. L. & Myszkowski, D. G. Higher-throughput, label-free, real-time molecular interaction analysis. *Anal. Biochem.* **361**, 1–6 (2007).
- Campbell, C. T. & Kim, G. SPR microscopy and its applications to high-throughput analyses of biomolecular binding events and their kinetics. *Biomaterials* **28**, 2380–2392 (2007).

44. Wang, S. & Guanxiong Li. Advances in giant magnetoresistance biosensors with magnetic nanoparticle tags: review and outlook. *IEEE Trans. Magnetics* **44**, 1687–1702 (2008).
45. Myszkka, D. G., He, X., Dembo, M., Morton, T. A. & Goldstein, B. Extending the range of rate constants available from BIAcore: interpreting mass transport-influenced binding data. *Biophys. J* **75**, 583–594 (1998).
46. Reichert, J. M. & Valge-Archer, V. E. Development trends for monoclonal antibody cancer therapeutics. *Nature Rev. Drug Discov.* **6**, 349–356 (2007).
47. Willett, C. G. *et al.* Direct evidence that the VEGF-specific antibody bevacizumab has antivasculature effects in human rectal cancer. *Nature Med.* **10**, 145–147 (2004).
48. Anderson, N. L. The clinical plasma proteome: a survey of clinical assays for proteins in plasma and serum. *Clin. Chem.* **56**, 177–185 (2010).
49. Cai, W. *et al.* Peptide-labeled near-infrared quantum dots for imaging tumor vasculature in living subjects. *Nano Lett.* **6**, 669–676 (2006).
50. Gaster, R. S., Hall, D. A. & Wang, S. X. Autoassembly protein arrays for analyzing antibody cross-reactivity. *Nano Lett.* doi:10.1021/nl1026056 (2010).
51. Srisa-Art, M., Dyson, E. C., deMello, A. J. & Edel, J. B. Monitoring of real-time streptavidin–biotin binding kinetics using droplet microfluidics. *Anal. Chem.* **80**, 7063–7067 (2008).
52. Barbosa, M. D., Chamberlain, A. K. & Desjarlais, J. R. Optimized proteins that target Ep-CAM. US patent 7,557,190 (2009), available via <http://go.nature.com/lbOXuD>
53. Hefta, L. J. F., Neumaier, M. & Shively, J. E. Kinetic and affinity constants of epitope specific anti-carcinoembryonic antigen (CEA) monoclonal antibodies for CEA and engineered CEA domain constructs. *Immunotechnology* **4**, 49–57 (1998).
54. Chen, Y. *et al.* Selection and analysis of an optimized anti-VEGF antibody: crystal structure of an affinity-matured fab in complex with antigen. *J. Mol. Biol.* **293**, 865–881 (1999).

Acknowledgements

This work was supported, in part, by the United States National Cancer Institute (grants 1U54CA119367, 1U54CA143907, 1U54CA151459 and N44CM–2009-00011), the United States National Science Foundation (grant ECCS-0801385-000), the United States Defense Advanced Research Projects Agency/Navy (grant N00014–02-1–0807), a Gates Foundation Grand Challenge Exploration Award and The National Semiconductor Corporation. R.S.G. acknowledges financial support from the Stanford Medical School Medical Scientist Training Program and a National Science Foundation graduate research fellowship. The authors thank M. Hammer and A. Bhattacharjee for editing the manuscript.

Author contributions

R.S.G. and S.X.W. designed the research. R.S.G. performed the research. R.S.G., R.J.W. and S.X.W. developed the model. R.S.G., L.X., S.H., R.J.W., D.A.H., S.J.O., H.Y. and S.X.W. contributed analytical tools. R.S.G., R.J.W. and S.X.W. analysed the data. S.J.O., L.X., S.H. and S.X.W. designed the magnetic sensor arrays. R.S.G. and H.Y. developed the biochemistry. R.S.G. and S.X.W. wrote the paper.

Additional information

The authors declare competing financial interests: details accompany the paper at www.nature.com/naturenanotechnology. Supplementary information accompanies this paper at www.nature.com/naturenanotechnology. Reprints and permission information is available online at <http://npg.nature.com/reprintsandpermissions/>. Correspondence and requests for materials should be addressed to S.X.W.